Electronic Supplementary Information

Transmetallation reactions of a Lithium Disilenide

Michael J. Cowley,[a] Kai Abersfelder,[a] Andrew J. P. White,[b] Moumita Majumdar[a] and David Scheschkewitz*[a]

[a)] Krupp-Chair of General and Inorganic Chemistry, University of Saarbrücken, D-66125 Saarbrücken, Germany

[b)] Imperial College London, Dept of Chemistry, London SW7 2AZ, UK

Content

General remarks

All procedures were carried out under an argon atmosphere, using standard Schlenk and glovebox techniques. Solvents were dried using Na/benzophenone and distilled under argon. C_6D_6 and d_8-toluene were dried over Na or K then distilled under Ar. $ZnCl_2$ (Aldrich) was dried by stirring in freshly distilled thionyl chloride for 16 hours. The bulk of the thionyl chloride was subsequently removed by distillation and then the $ZnCl_2$ was dried thoroughly in vacuo before use. $Tip_2Si{=}Si(Tip)Li{\cdot}2Et_2O$ (**1**) was prepared according to the published procedure.[1]

UV/Vis spectra were acquired using a Perklin-Elmer Lambda 35 spectrometer using quartz cells with a path length of 0.1 cm. NMR spectra were recorded on a Bruker Avance III 300 MHz spectrometer. ^{1}H and ^{13}C spectra were referenced to residual solvent resonances and ^{29}Si NMR to an external reference (tetramethylsilane).

Synthesis of 1,1,2-tris(2',4',6'- triisopropylphenyl)disilenylmagnesium bromide **3**

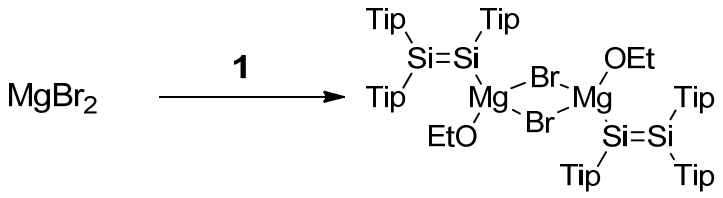

3

At room temperature, magnesium turnings (1.07 g, 44.01 mmol) were suspended in diethyl ether (20 mL). A solution of dibromoethane (8.15 g, 43.38 mmol) in diethyl ether (30 mL) was added dropwise over 25 minutes, maintaining the solution at a gentle reflux. After cooling back to room temperature, solution of **1** (2.01 g, 2.36 mmol) in diethyl ether (30 mL) was added dropwise. The initially orange reaction mixture became a yellow suspension after stirring for 3 h. After 6 h, all volatiles were removed in vacuo and the residue was digested with toluene (70 mL). Insoluble material was removed by filtration and the filtrate was reduced to dryness yielding 1.78 g (1.03 mmol, 88%) **2**·C_7H_8 as yellow solid. Compound **2** was recrystallized from a concentrated hexane solution at room temperature, yielding x-ray quality crystals in 46% yield (mp. 203 °C, dec.).

^{1}H NMR (500.13 MHz, C_6D_6, 25 °C): δ = 7.04, 7.03, 6.98 (each s, altogether 6H, Tip-*H*), 4.57, 4.38, 3.94 (each br., altogether 6H, iPr-C*H*), 3.22 (br, 4H, Et_2O-CH_2), 2.78, 2.73, 2.71 (each hept., altogether 3H, iPr-C*H*), 1.41 (br., 18H, iPr-CH_3), 1.23, 1.17, 1.14 (each d, altogether 18H, iPr-CH_3), 1.11, 1.03 (each br., altogether 18H, iPr-CH_3), 0.64 (br, 6H, Et_2O-CH_3).
^{13}C{^{1}H} NMR (125.76 MHz, C_6D_6, 25 °C): δ = 155.11, 154.90, 154.39 (br.), 149.80, 149.46, 147.78, 138.85, 138.71, 137.85 (Tip-*C*), 121.90, 121.34, 120.94 (Tip-*C*H), 65.67 (Et_2O-*C*H_2), 37.18, 36.54, 36.03 (br.), 34.90, 34.71, 34.52 (iPr-*C*H), 27.64 (br.), 25.40 (br.), 24.72, 24.41, 24.28, 24.06, 23.96 (br.) (iPr-*C*H_3), 13.63 (Et_2O-*C*H_3).
^{29}Si{^{1}H} NMR (99.36 MHz, C_6D_6, 25 °C): δ = 111.3 (*Si*Tip_2), 59.5 (*Si*TipMg).
UV/Vis (hexane) l_{max} (e) = 425 nm (4193 $Lmol^{-1}cm^{-1}$).
MS (EI) *m/z* (%) = 435.3 (47.0), 230.1 (100.0), 204.2 (19.6), 189.1 (61.7), 161.1 (20.9), 95.0 (25.2), 43.0 (18.5).

[S1] Scheschkewitz, D. *Angew. Chem. Int. Ed.* **2004**, *43*, 2965.

Synthesis of [lithium tris(dimethoxyethane)] [bis(1,1,2-tris(2',4',6'-triisopropylphenyl)disilenyl)cuprate] **4**

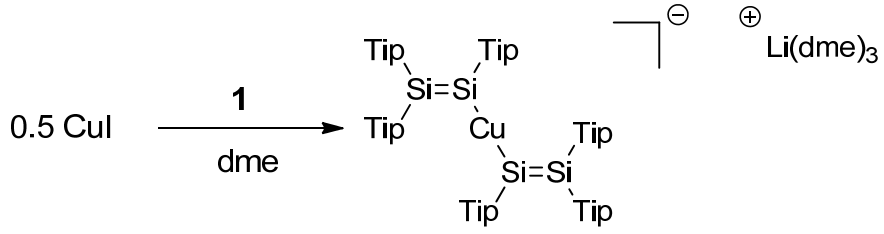

4

At room temperature, CuI (112 mg, 0.586 mmol) and **1** (1.00 g, 1.172 mmol) were dissolved in dimethoxyethane (20 mL). The dark red/purple solution was stirred at room temperature for 1.5 hours. The solvent was removed in vacuo and the red, solid residue was dissolved in hexane (40 mL). The hexane solution was filtered immediately and the filtrate stored at room temperature for 2 days. Deep red crystals of **4** were separated by filtration and dried in vacuo. Yield 816 mg, 83 %. (mp. 176 °C, dec.).

^{1}H NMR (300.13 MHz, d_8-THF, 300 K): δ = 6.76 (s, 4H, Si($C_6H_2^iPr_3$)$_2$), 6.65 (s, 4H. Si(Cu)($C_6H_2^iPr_3$), 6.64 (s, 4H, Si($C_6H_2^iPr_3$)$_2$), 4.46 (sept, $^3J_{HH}$ = 6.8 Hz, 4H, C*H*(CH_3)$_2$)., 4.31 (br, 4H, C*H*(CH_3)$_2$), 3.80 (br, 4H, C*H*(CH_3)$_2$), 3.42 (s, 12H, dme CH_2), 3.25 (s, 18H, dme CH_3), 2.73 (sept, $^3J_{HH}$ = 6.9 Hz, 2H, C*H*(CH_3)$_2$), 2.65 (sept, $^3J_{HH}$ = 6.8 Hz, 2H, C*H*(CH_3)$_2$), 2.64 (sept, $^3J_{HH}$ = 6.8 Hz, 2H C*H*(CH_3)$_2$), 1.18 (d, $^3J_{HH}$ = 6.9 Hz, 12H, CH(CH_3)$_2$), 1.16 (br d, $^3J_{HH}$ = 6 Hz, 12H, CH(CH_3)$_2$), 1.12 (d, $^3J_{HH}$ = 6.9 Hz, 12H, CH(CH_3)$_2$), 1.07 (d, $^3J_{HH}$ = 6.9 Hz, 12H, CH(CH_3)$_2$), 0.97 (br d, $^3J_{HH}$ = 6.6 Hz, 12H, CH(CH_3)$_2$), 0.85 (br d, $^3J_{HH}$ = 5.0 Hz, 12H, CH(CH_3)$_2$), 0.74 (br, 12H, CH(CH_3)$_2$), 0.59 (br, 24H, CH(CH_3)$_2$).

^{13}C{^{1}H} NMR (125.76 MHz, C_6D_6, 25 °C): δ = 155.16, 155.12, 154.61, 150.49, 150.45, 149.02, 137.20, 136.60, 134.75 (Tip-*C*), 122.03, 121.99, 121.37 (Tip-*C*H), 37.58, 36.76, 35.20, 35.09, 34.85 (iPr-*C*H), 24.86, 24.59, 24.35, 24.21, 24.16, 23.94, 23.67 ((iPr-CH_3).

^{29}Si{^{1}H} NMR (59.62 MHz, d_8-THF, 300 K): δ = 94.46 (*Si*TipCu), 90.16 (*Si*Tip$_2$).

^{29}Si{^{1}H} NMR (59.62 MHz, C_6D_6, 300 K): δ = 93.6 (*Si*TipCu), 91.8 (*Si*Tip$_2$).
The cuprate **4** slowly decomposes in C_6D_6 to unidentified products; complete NMR spectroscopic analysis was carried out in d_8-THF.

UV/Vis (THF) λ_{max} (ε) = 476 nm (31,127 L mol^{-1}cm^{-1}), 371 nm.

UV/Vis (hexane) λ_{max} (ε) = 462 nm, 384 nm.
The limited solubility of **4** in hexane rendered quantitative analysis problematic, which was therefore carried out in THF.

Elemental Analysis calculated for $C_{102}H_{168}Si_4CuLiO_6$: C, 73.23 ; H, 10.12 . Found: C, 73.10; H, 10.20

Synthesis of bis(1,1,2-tris(2',4',6'-triisopropylphenyl)disilenyl)zinc **5**

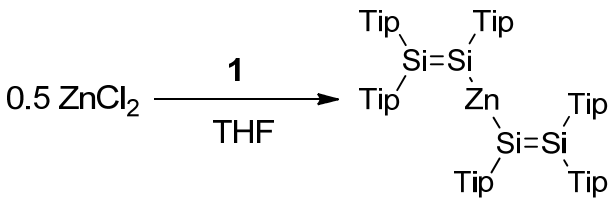

5

At room temperature, a solution of $ZnCl_2$ (80 mg, 0.586 mmol) in THF (20 mL) was added rapidly to a solution of **1** (1.00 g, 1.172 mmol) in THF (20 mL). The resulting mixture was stirred for 2 hours. The solvent was then removed in vacuo and the red, solid residue was dissolved in hexane (40 mL) and filtered. The filtrate was concentrated to a volume of 10 mL before benzene (10 mL) was added to the solution. Compound **5** precipitated as a red solid and was isolated by filtration. Yield 408 mg, 50 %. (mp. 204 °C, dec.).

^{1}H NMR (300.13 MHz, d_8-THF, 300 K): δ = 6.93 (s, 4 H, Si(Zn)($C_6H_2{}^iPr_3$)), 6.79 (s, 8 H, Si($C_6H_2{}^iPr_3$)$_2$), 4.07 (sept, $^3J_{H-H}$ = 6.8 Hz, 4H, C*H*(CH_3)$_2$), 4.01 (br, 4H, C*H*(CH_3)$_2$), 3.52 (br sept, 4H, C*H*(CH_3)$_2$), 2.79 (sept, $^3J_{H-H}$ = 6.9 Hz, 2H, C*H*(CH_3)$_2$), 2.70 (sept, $^3J_{H-H}$ = 6.9 Hz, 2H, C*H*(CH_3)$_2$), 2.69 (sept, $^3J_{H-H}$ = 6.9 Hz, 2H, C*H*(CH_3)$_2$), 1.19 (d, $^3J_{H-H}$ = 6.9 Hz, CH(C*H*$_3$)$_2$) 1.16 (br, CH(C*H*$_3$)$_2$), 1.13 (d, 12 H, $^3J_{H-H}$ = 6.9 Hz, CH(C*H*$_3$)$_2$), 1.09 (d, 12 H, $^3J_{H-H}$ = 6.9 Hz, CH(C*H*$_3$)$_2$), 0.94, 0.87 (br, 36 H, CH(C*H*$_3$)$_2$), 0.68 (br, 24 H, CH(C*H*$_3$)$_2$).

^{13}C{^{1}H} NMR (75.47 MHz, d_8-THF, 300 K): δ = 154.13, 153.59, 146.92, 146.40, 144.92, 143.35, 141.25, 140.78 (Tip-*C*), 120.08, 119.92, 119.02 (Tip-*C*H), 71.75 (dme *C*H$_2$), 57.93 (dme CH$_3$), 35.93 (br), 35.45 (br), 35.02 (br), 34.44, 34.35, 34.13 (^{i}Pr-*C*H), 26.79, 24.96, 23.74, 23.67, 23.45, 23.08, 22.82 (^{i}Pr-*C*H$_3$)

^{29}Si{^{1}H} NMR (59.62 MHz, d_8-THF, 300 K): δ = 107.05 (*Si*(Tip)Zn), 57.48 (*Si*Tip$_2$).

UV/Vis: (hexane) λ_{max} (ε) = 468 nm (28,728 L mol^{-1}cm^{-1}), 356 nm.

Elemental Analysis: calculated for $C_{90}H_{138}Si_4Zn$: C, 77.33 %; H, 9.95 %. Found: C, 76.72; H, 9.66

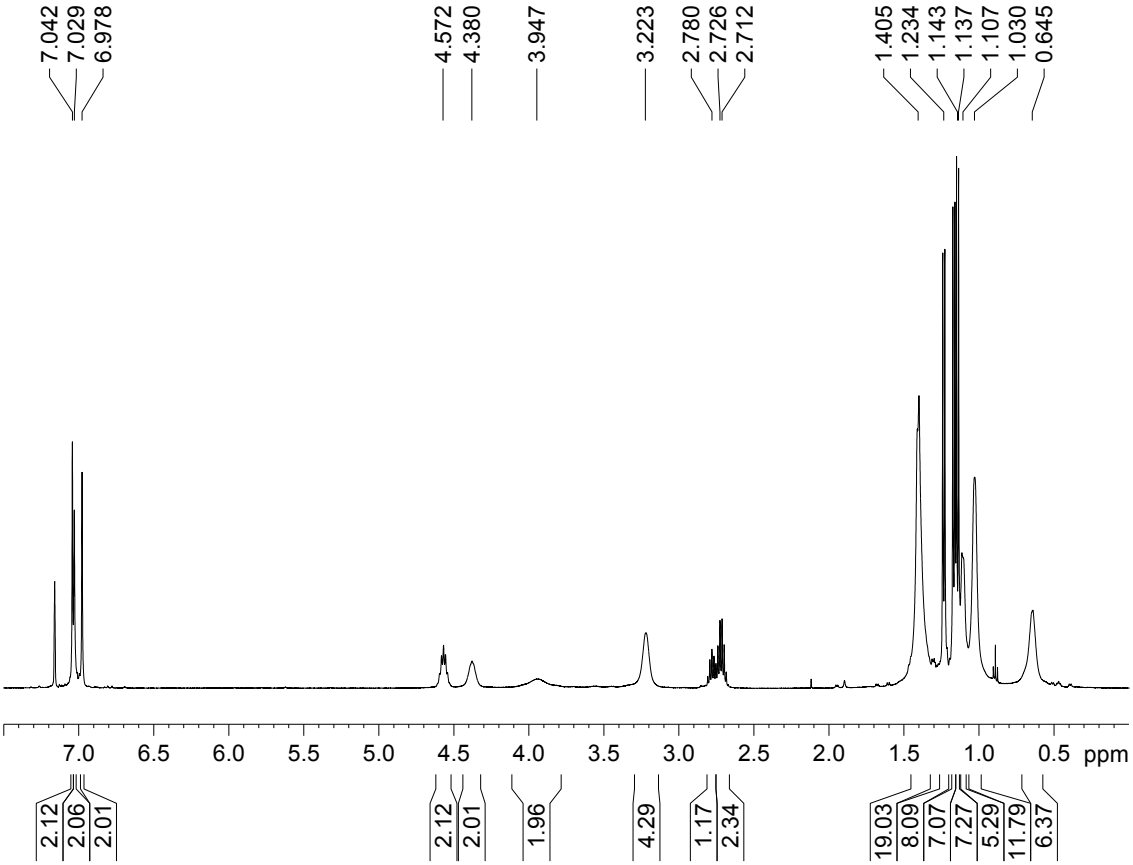

Fig. S1: ^{1}H NMR of **3** (benzene-d_6, 298K)

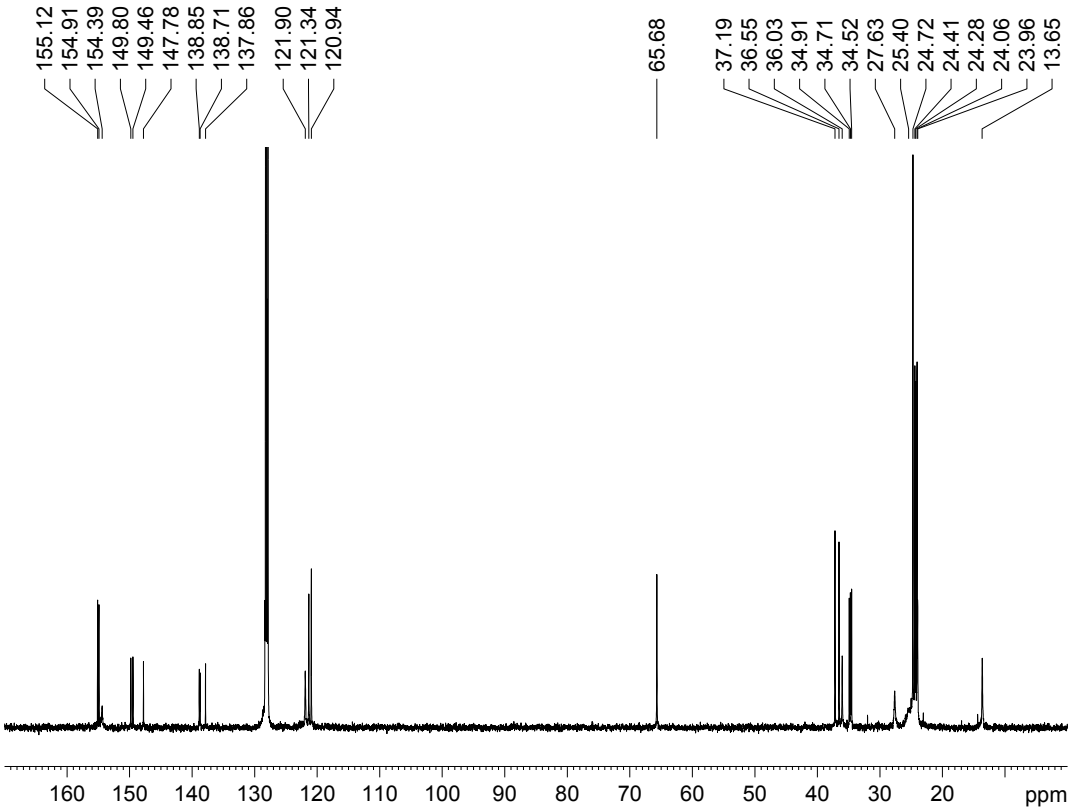

Fig. S2: ^{13}C{^{1}H} NMR of **3** (benzene-d_6, 298K)

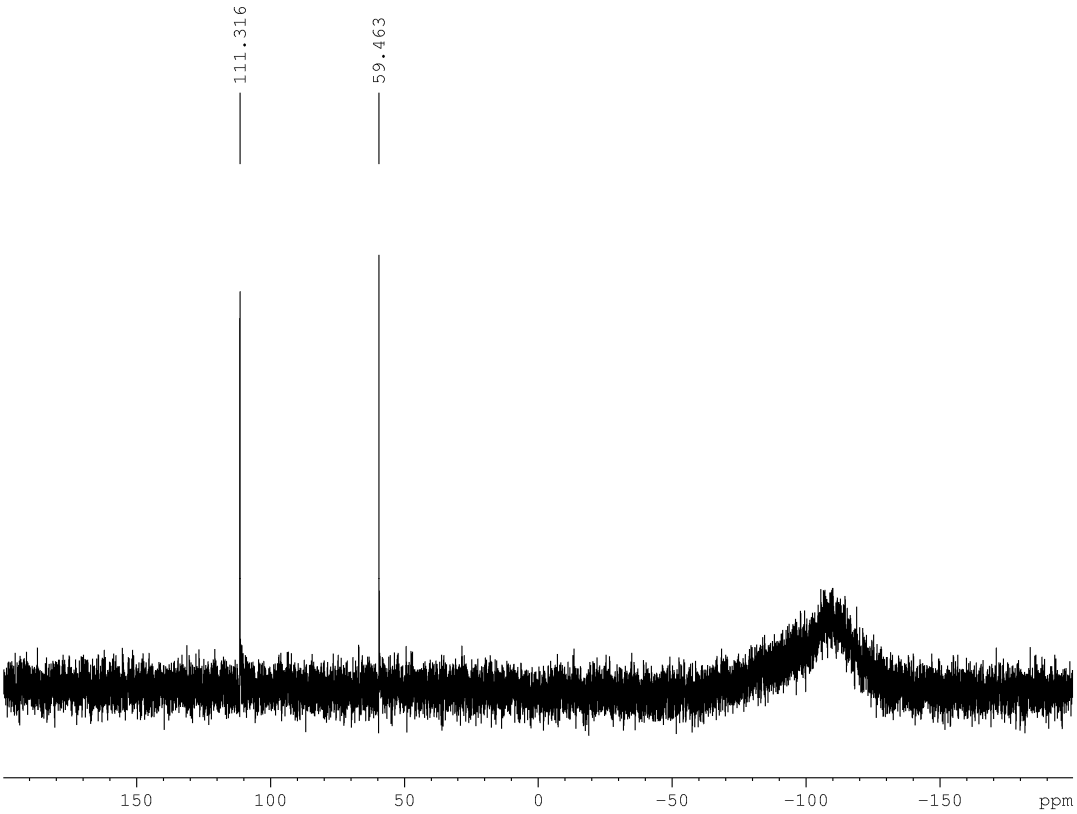

Fig. S3: ^{29}Si NMR of **3** (benzene-d_6, 298K)

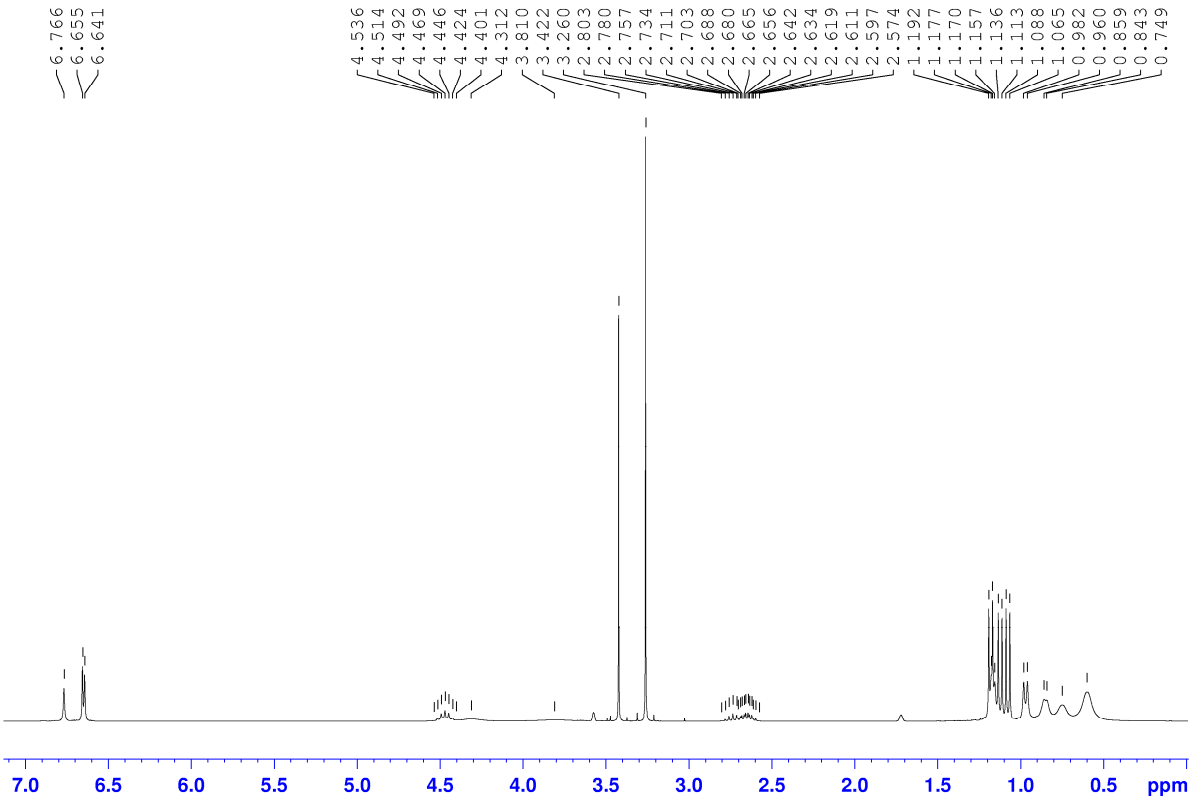

Fig. S4: ^{1}H NMR of **4** (thf-d_8, 298K)

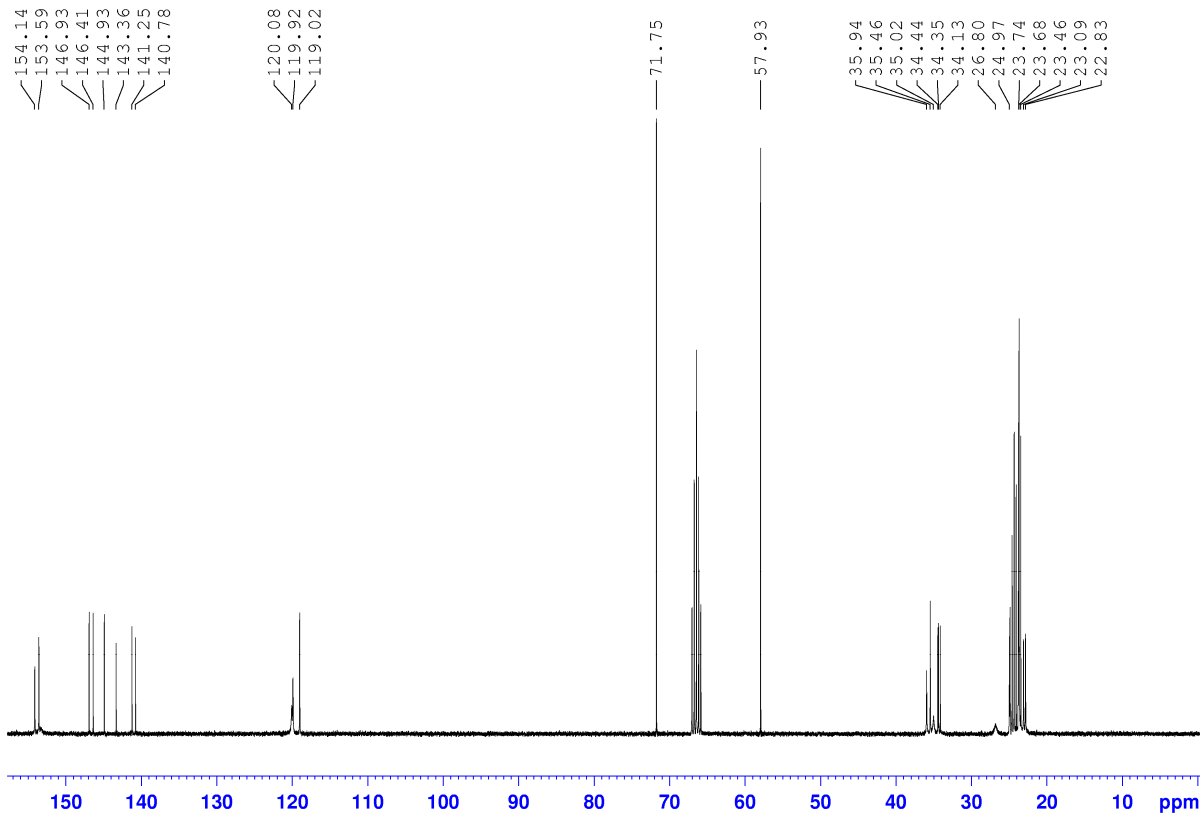

Fig. S5: $^{13}C\{^{1}H\}$ NMR of **4** (thf-d_8, 298K)

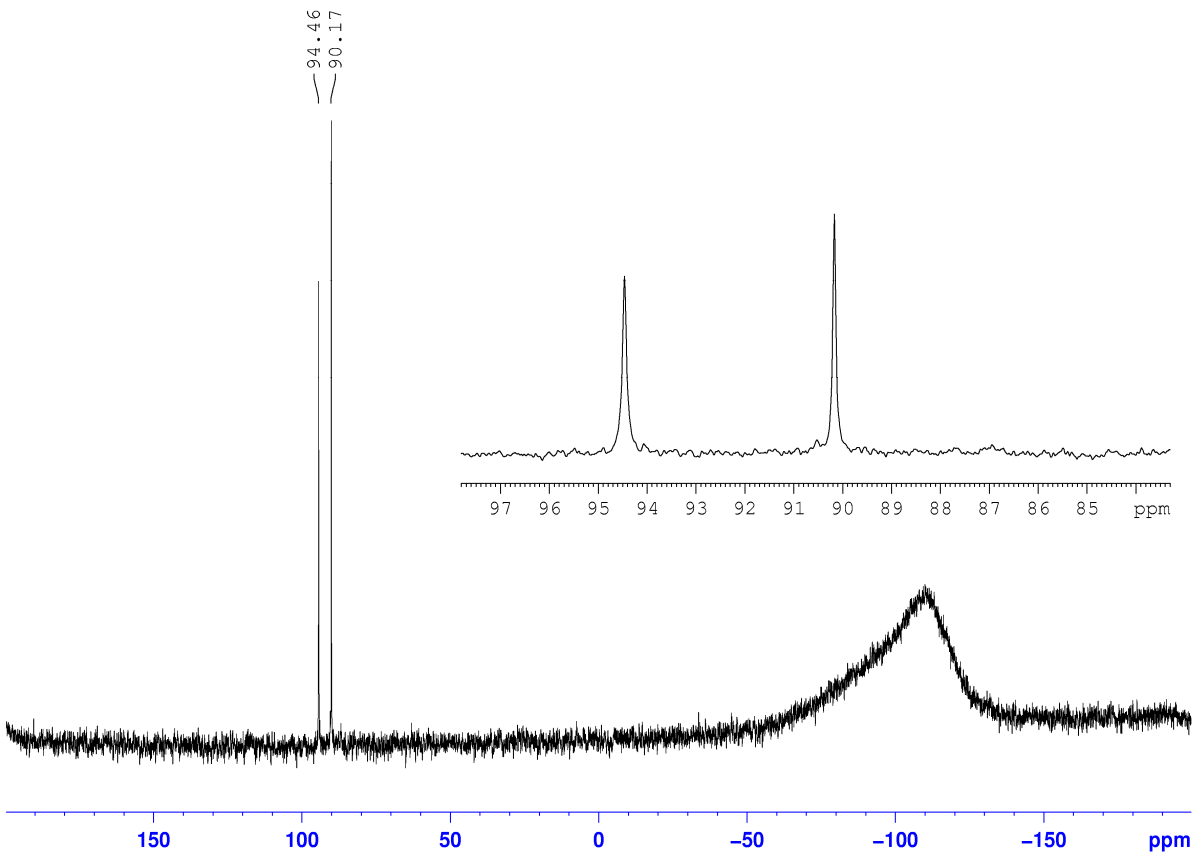

Fig. S6: ^{29}Si NMR of **4** (thf-d_8, 298K)

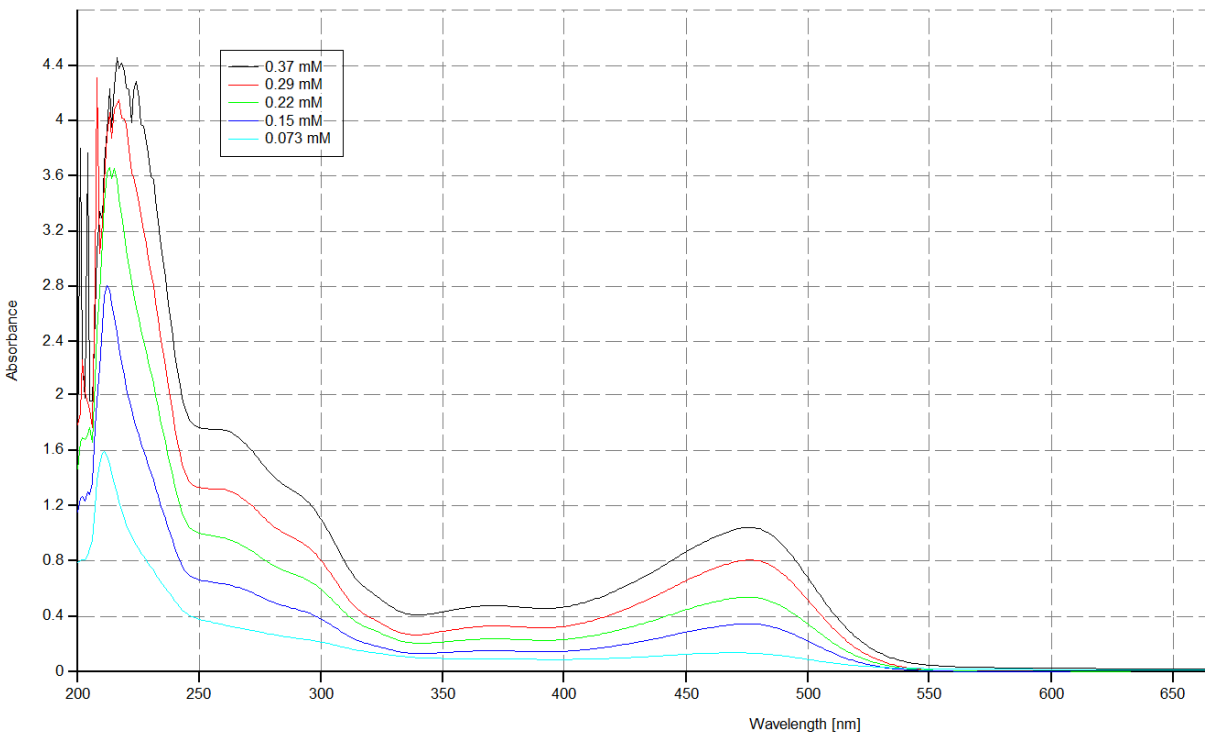

Fig. S7: UV-vis of **4** (thf, 298K)

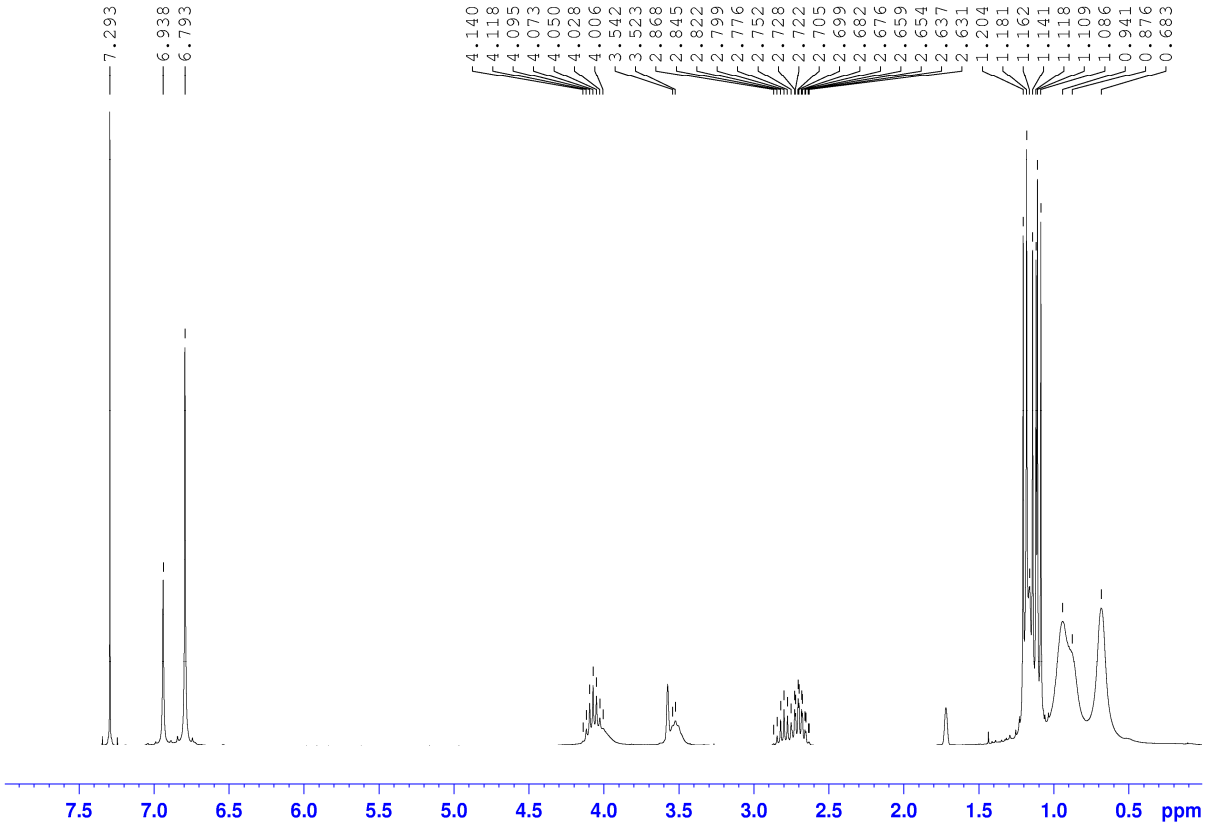

Fig. S8: ^{1}H NMR of **5** (thf-d_8, 298K)

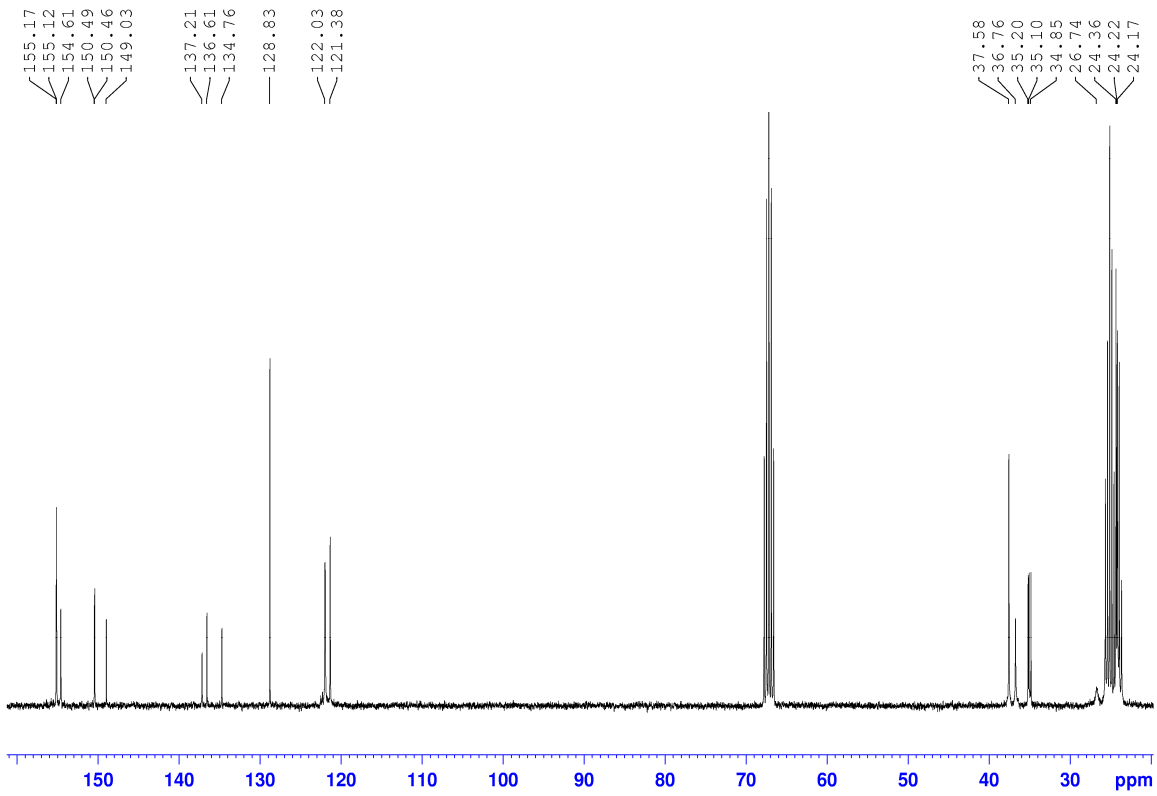

Fig. S9: $^{13}C\{^{1}H\}$ NMR of **5** (thf-d_8, 298K)

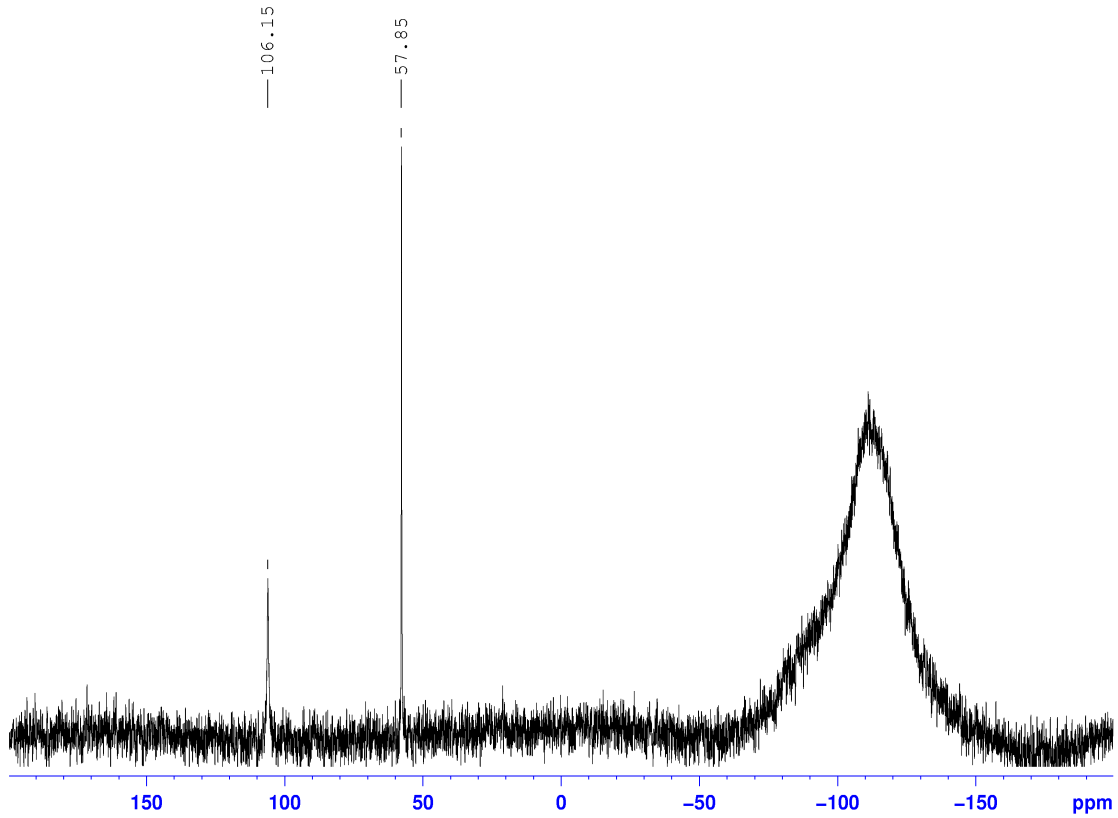

Fig. S10: ^{29}Si NMR of **5** (thf-d_8, 298K)

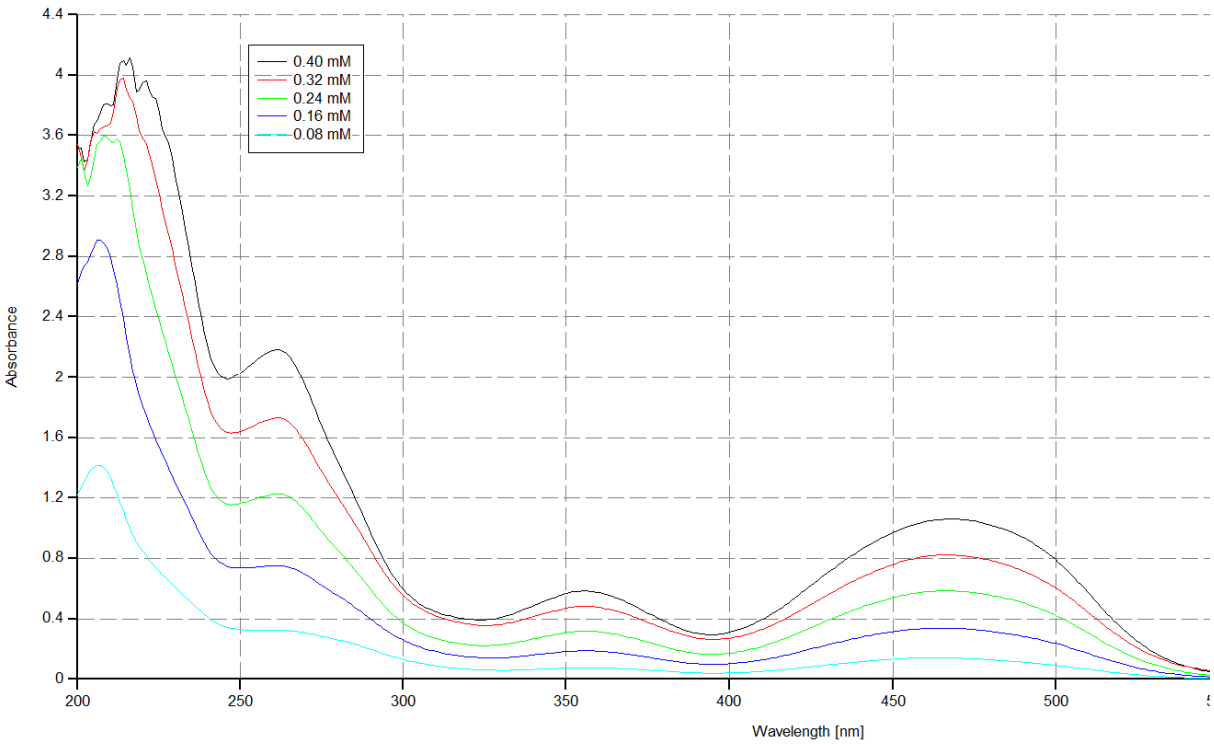

Fig. S11: UV-vis of **5** (hexane, 298K)

X-Ray Crystal Structure of **3**

No significant disorder was observed so that standard refinement proceeded smoothly with anisotropic treatment of all heavy atoms.

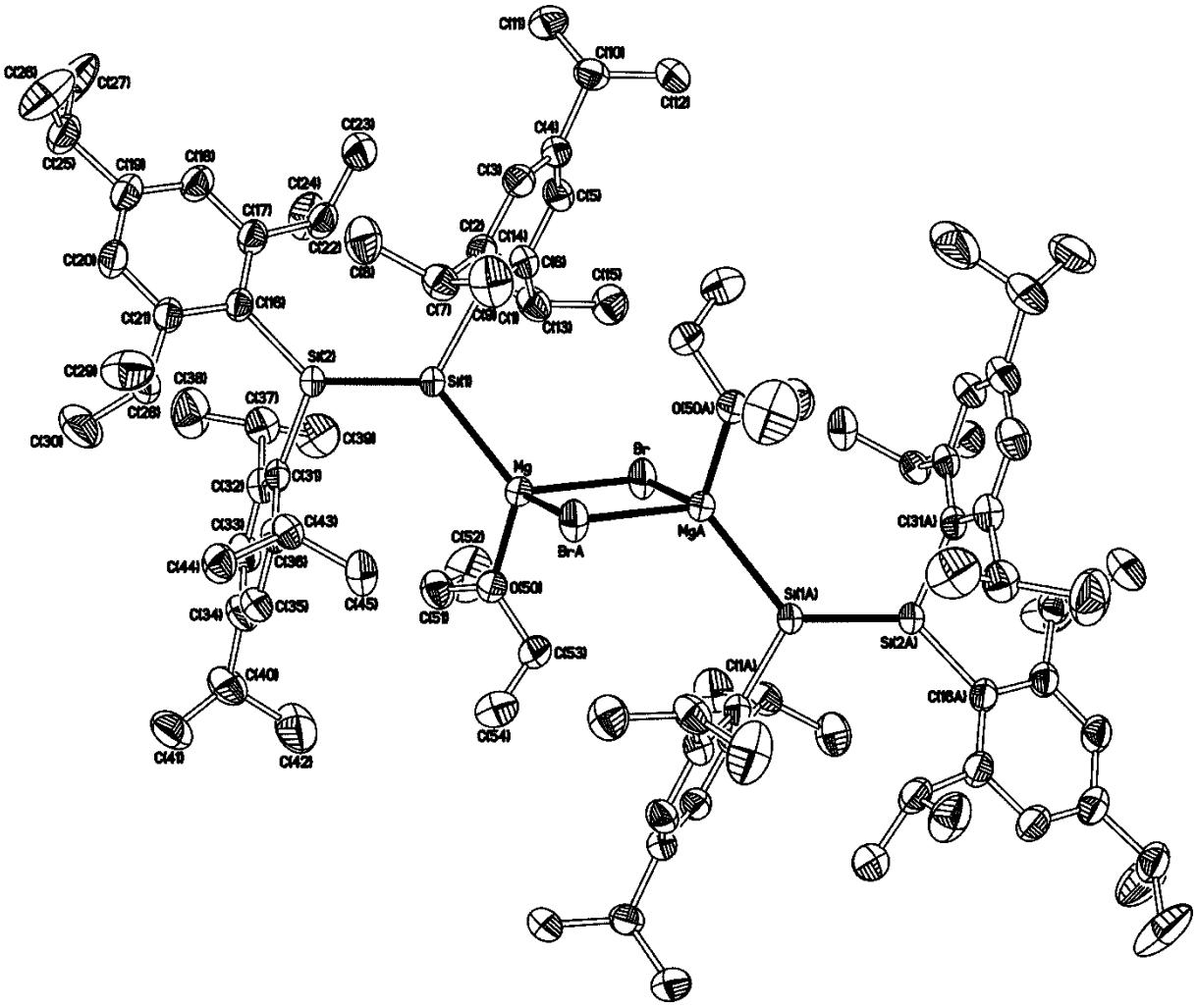

Fig. S12 ORTPEP plot of the structure of **3** in the solid state with complete numbering scheme

X-ray crystal structure of **4**

The C(10)- and C(40)-based isopropyl groups were found to be disordered. In both cases two orientations were identified for the whole group, with orientations of ca. 61:39 and 55:45% respectively. The geometries of all four orientations were optimised, the thermal parameters of adjacent atoms restrained to be similar, and only the major occupancy non-hydrogen atoms were refined anisotropically.

The O(102)/O(105) based 1,2-dimethoxyethane ligand of the $[Li(dme)3]^+$ cation was found to be disordered. Two orientations were identified for the whole ligand of ca. 66 and 34% occupancy respectively. The geometries of the two orientations were optimised, the thermal parameters of adjacent atoms restrained to be similar, and only the major occupancy non-hydrogen atoms were refined anisotropically.

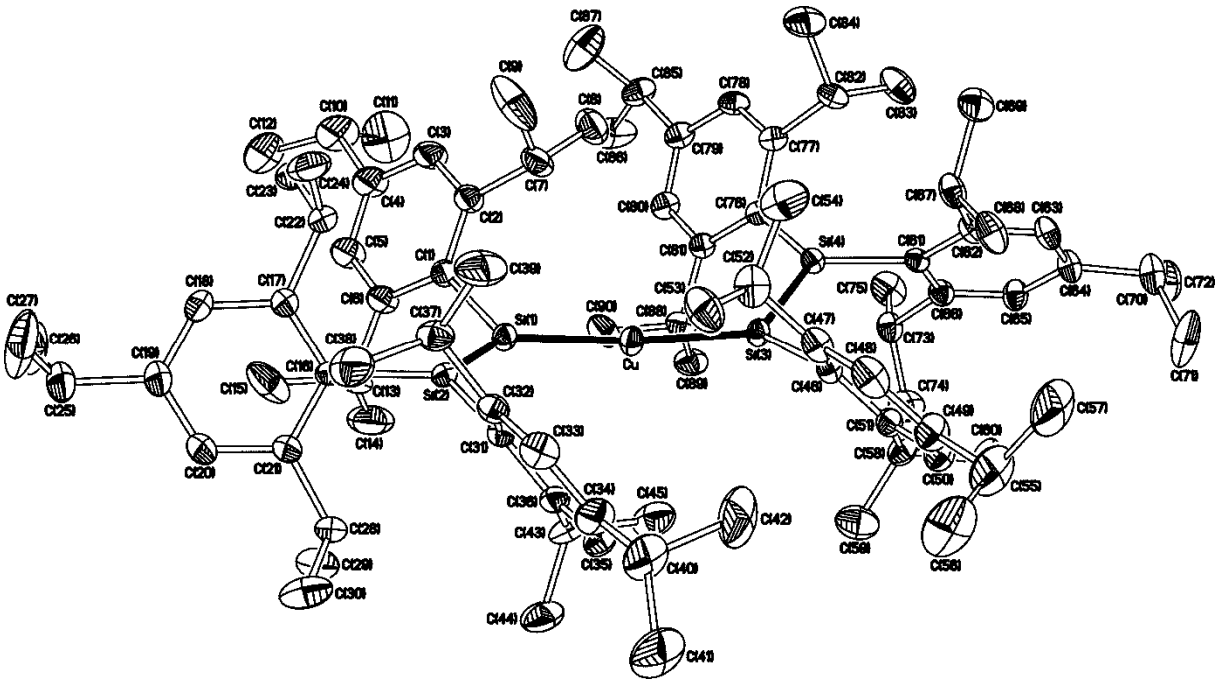

Fig. S13 ORTEP plot of the structure of the anionic part of **4** in the solid state with complete numbering scheme

TD-DFT calculations of **A**, **B**, **4Ph** and **5Ph**

In order to elucidate the origin of the UV-vis absorption bands of compounds **4** and **5**, TD-DFT calculations were performed at the B3LYP level (using 6-31G(d, p) for C, H, Si, and LANL2DZ basis set for Cu and Zn atoms). The simplified model systems **4Ph** and **5Ph** were considered (Ph instead of Tip) using the X-ray coordinates of **4** and **5** without optimization (Scheme S1). Heptane was chosen as the solvent in Tomasi's Polarized Continuum Model (PCM). The Gaussian 03 suite of programs was employed in all calculations.[S2]

For comparison, the truncated model systems (Ph instead of Tip) of tetraphenyldisilene **A** and *p*-phenylene bridged tetrasiladiene **B** were also calculated. Again, the experimental geometry of compounds **6** and **7** of our previous publication was used without optimization.[S3]

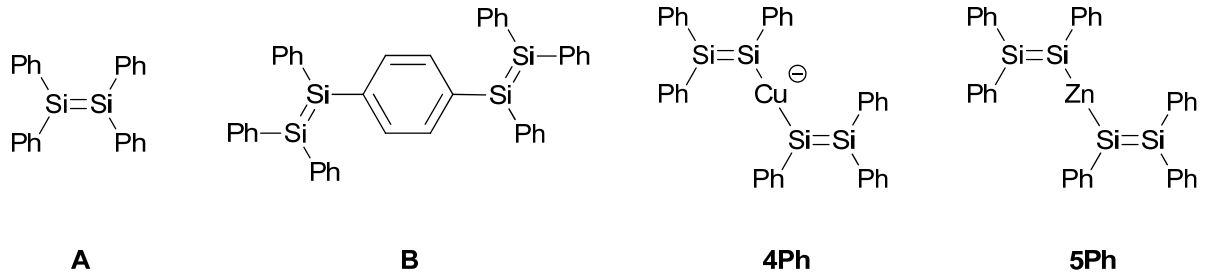

Scheme S1 Compounds subject to TD-DFT studies.

The simulated spectrum of **4Ph** (Fig. S14) shows two intense absorption peaks at λ_{max} = 504 nm (f = 0.5834, HOMO→LUMO) and 391 nm (f = 0.1856, HOMO−1→LUMO+1), which are significantly red-shifted compared to the experimental values of λ_{max} = 476 and 371 nm. Conversely, in case of neutral **5Ph** (Fig. S15), the simulated spectrum shows two intense absorption peaks at λ_{max} = 464 nm (f = 0.5855, HOMO→LUMO) and 358 nm (f = 0.3705, HOMO−1→LUMO+1 and HOMO−1→LUMO+2), in excellent agreement with the experimental bands at λ_{max} = 468 and 356 nm.

The calculated longest wavelength absorptions for compounds **A** and **B** are at 407 nm (f = 0.4507, HOMO→LUMO) and 501 nm (f = 0.9508, HOMO→LUMO), respectively, in reasonable agreement with the experimental values and thus corroborating our suspicion that the absence of the counter cation in the TD-DFT computation of **4Ph** is responsible for the pronounced deviation from experimental data.

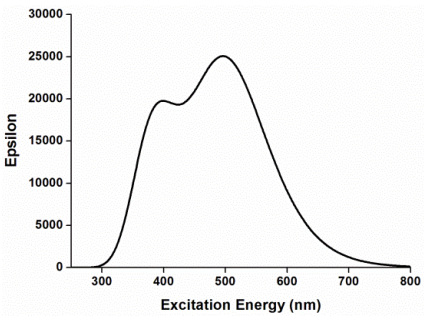

Fig. S14 Calculated UV-vis spectra of **4Ph**.

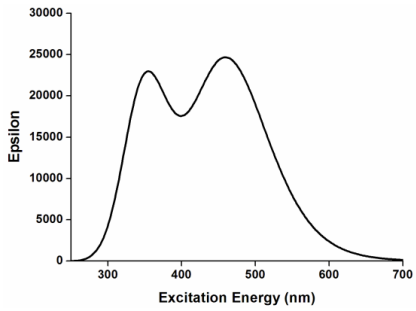

Fig. S15 Calculated UV-vis spectra of **5Ph.**

The schematic comparison of orbital energies in Fig. S16 shows two pertinent features: the raising of orbital energies due to the presence of a negative charge in **4Ph** and the decreased HOMO-LUMO gap in both **4Ph** and **5Ph** compared to **A**, i.e. a compound with just one isolated Si=Si bond.

[S2] Frisch, M. J.; et al. *Gaussian 03*, revision E.01; Gaussian Inc.: Wallingford, CT, 2004.
[S3] Bejan, I.; Scheschkewitz, D. *Angew. Chem. Int. Ed*. **2007**, *46*, 5783.

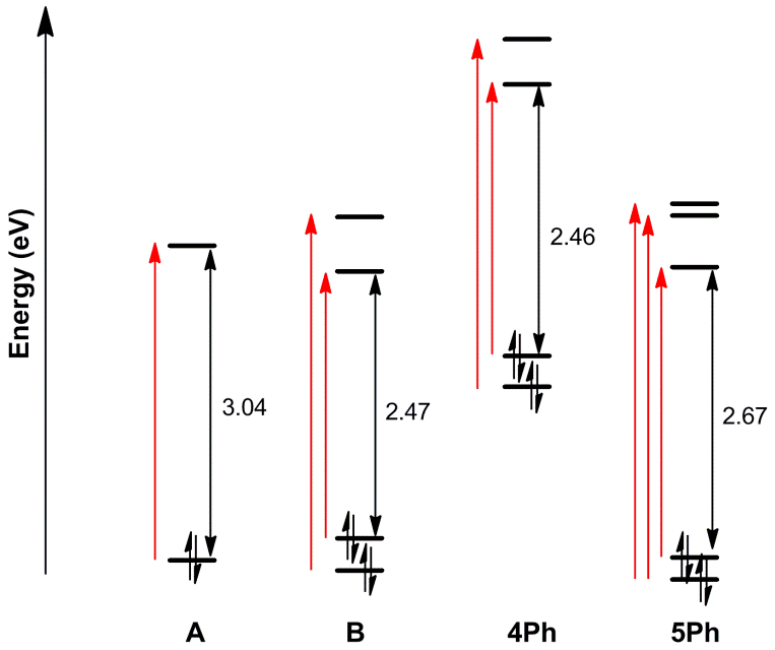

Fig. S16 Relevant transitions in **A**, **B**, **4Ph** and **5Ph**.

The relevant MOs of **A**, **B**, **4Ph** and **5Ph** are shown in Fig. S17 and S18. In all cases, the HOMO is primarily represented by the π(Si=Si) orbital and the LUMO involves the π*(Si=Si) orbital. In **4Ph**, the overall anionic charge raises the energy of the system, resulting in the interaction of Cu d orbitals with the frontier π(Si=Si) orbitals. The HOMO is destabilized due to the admixture of the Cu d_{xz} orbital in an anti-bonding interaction, which explains the red-shift of the longest wavelength absorption with respect to **A**. On the other hand, in the neutral **5Ph**, the low-lying Zn d orbitals contributes only marginally to the frontier π(Si=Si) orbitals. The $4p_z$ orbital of Zn (with admixture of metal s orbital) shows bonding overlap with the π*(Si=Si) in the LUMO, thereby stabilizing it, which explicitly explains the bathochromic shift of the longest wavelength absorption compared to the disilene **A** with an isolated Si=Si moiety. This MO also reflects the π-conjugation over the Si=Si-Zn-Si=Si framework. A similar situation is encountered in the conjugated, para-phenylene bridged **B** with two Si=Si moieties, which exhibits the strongest bathochromic shift among the series. In this case, the LUMO is stabilized by bonding overlap of π*(Si=Si) with the phenylene ring.

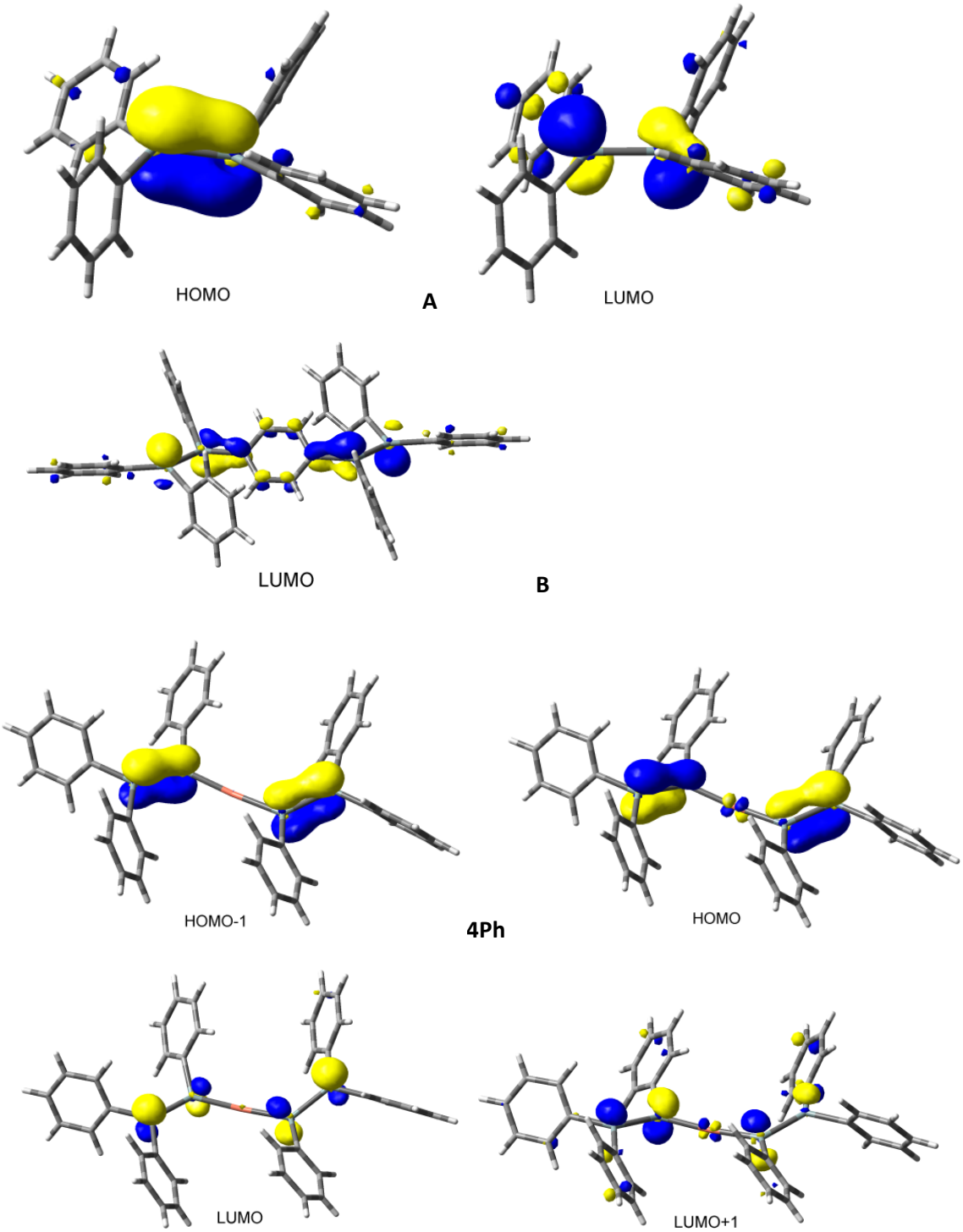

Fig. S17. Selected MOs of **A**, **B** and **4Ph**.

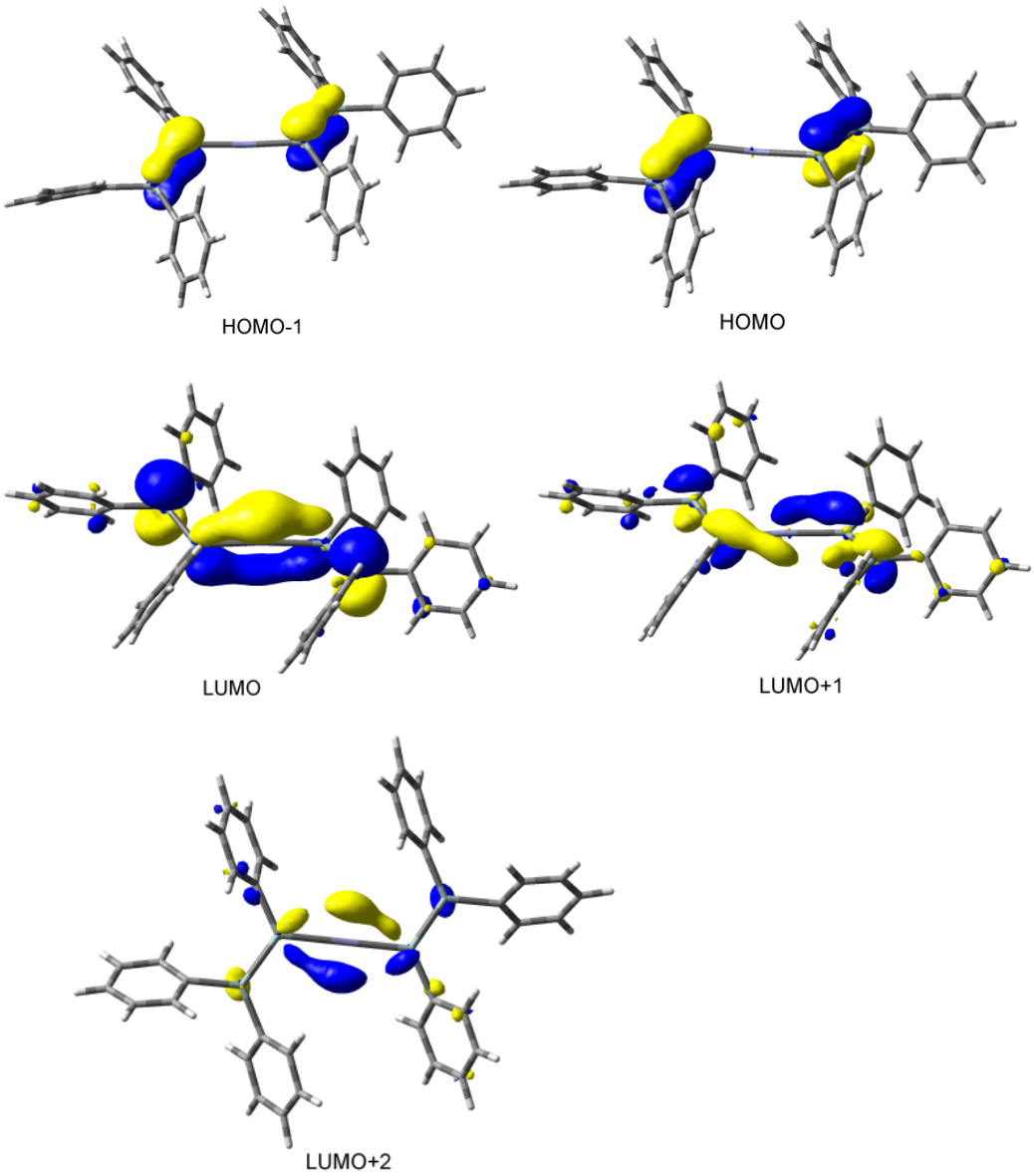

Figure S18. Selected MOs of **5Ph**.

TD-DFT output excerpts

4Ph:

```
Excitation energies and oscillator strengths:

 Excited State   1:   Singlet-A      2.4583 eV  504.35 nm  f=0.5834
     161 ->162         0.65076
 This state for optimization and/or second-order correction.
 Copying the excited state density for this state as the 1-particle
RhoCI density.

 Excited State   2:   Singlet-A      2.7469 eV  451.36 nm  f=0.0010
     160 ->162         0.57611
     161 ->163        -0.38995

 Excited State   3:   Singlet-A      2.8950 eV  428.26 nm  f=0.0111
     160 ->162        -0.22752
     160 ->164         0.12035
     161 ->163        -0.30112
     161 ->164         0.51229
     161 ->165        -0.12209

 Excited State   4:   Singlet-A      2.9756 eV  416.67 nm  f=0.0071
     160 ->162         0.20616
     160 ->167        -0.10453
     161 ->163         0.43269
     161 ->164         0.35061
     161 ->165        -0.14087

 Excited State   5:   Singlet-A      3.0184 eV  410.76 nm  f=0.1035
     160 ->164         0.28072
     161 ->164         0.16169
     161 ->165         0.59300

 Excited State   6:   Singlet-A      3.0978 eV  400.23 nm  f=0.0126
     159 ->162         0.64446
     160 ->163         0.17335

 Excited State   7:   Singlet-A      3.1303 eV  396.08 nm  f=0.0092
     160 ->163         0.13854
     160 ->165        -0.25365
     161 ->166         0.60741

 Excited State   8:   Singlet-A      3.1733 eV  390.71 nm  f=0.1856
     159 ->162        -0.12401
     160 ->163         0.43578
     160 ->167         0.12365
     161 ->167        -0.40321
     161 ->169        -0.16718
     161 ->170        -0.11282

 Excited State   9:   Singlet-A      3.2534 eV  381.09 nm  f=0.0474
     159 ->162        -0.15776
     160 ->163         0.28306
     160 ->164        -0.29037
```

```
     160 ->165         0.18427
     160 ->166        -0.29031
     161 ->165         0.15409
     161 ->167         0.14385
     161 ->169         0.31308

 Excited State  10:   Singlet-A      3.3029 eV  375.38 nm  f=0.0791
     160 ->163         0.27482
     160 ->166         0.14607
     160 ->167        -0.18598
     161 ->166        -0.12470
     161 ->167         0.46035
     161 ->169        -0.29292
```

5Ph:

```
Excitation energies and oscillator strengths:

 Excited State   1:   Singlet-B      2.6731 eV  463.82 nm  f=0.5855
     157 ->158         0.65539
 This state for optimization and/or second-order correction.
 Copying the excited state density for this state as the 1-particle
RhoCI density.

 Excited State   2:   Singlet-A      2.8444 eV  435.88 nm  f=0.0003
     156 ->158         0.39012
     157 ->159         0.48043
     157 ->160        -0.32069

 Excited State   3:   Singlet-A      2.8931 eV  428.55 nm  f=0.0002
     156 ->158         0.51072
     157 ->159        -0.14755
     157 ->160         0.42579

 Excited State   4:   Singlet-B      3.0642 eV  404.63 nm  f=0.0208
     156 ->159        -0.48524
     156 ->160         0.49488

 Excited State   5:   Singlet-B      3.2591 eV  380.42 nm  f=0.0451
     155 ->158         0.68470

 Excited State   6:   Singlet-A      3.2975 eV  375.99 nm  f=0.0062
     155 ->159         0.11109
     156 ->158        -0.12853
     157 ->159         0.43821
     157 ->160         0.42880

 Excited State   7:   Singlet-B      3.4675 eV  357.56 nm  f=0.3705
     156 ->159         0.44738
     156 ->160         0.46680
     157 ->163        -0.13640

 Excited State   8:   Singlet-B      3.6322 eV  341.34 nm  f=0.0971
     156 ->162         0.32501
     157 ->161         0.61676
```

```
 Excited State   9:   Singlet-A      3.6330 eV  341.28 nm  f=0.0006
     156 ->161         0.33110
     157 ->162         0.61505

 Excited State  10:   Singlet-B      3.7400 eV  331.51 nm  f=0.0764
     156 ->159         0.11437
     156 ->165        -0.11342
     157 ->163         0.65826
```

A:

```
Excitation energies and oscillator strengths:

 Excited State   1:   Singlet-A      3.0460 eV  407.04 nm  f=0.4507
      96 -> 97         0.59018
      96 -> 98         0.17355
      96 ->100         0.11707
 This state for optimization and/or second-order correction.
 Copying the excited state density for this state as the 1-particle
RhoCI density.

 Excited State   2:   Singlet-A      3.3965 eV  365.03 nm  f=0.1085
      96 -> 97        -0.14088
      96 -> 98         0.67285

 Excited State   3:   Singlet-A      3.6260 eV  341.94 nm  f=0.0207
      96 -> 99         0.69592

 Excited State   4:   Singlet-A      3.9436 eV  314.39 nm  f=0.0659
      96 ->100         0.65449
      96 ->103        -0.12937

 Excited State   5:   Singlet-A      4.0485 eV  306.25 nm  f=0.0011
      96 ->101         0.67219
      96 ->102        -0.14938
```

B:

```
Excitation energies and oscillator strengths:

 Excited State   1:   Singlet-AU     2.4738 eV  501.19 nm  f=0.9508
     171 ->172         0.65063
 This state for optimization and/or second-order correction.
 Copying the excited state density for this state as the 1-particle
RhoCI density.

 Excited State   2:   Singlet-AG     2.7830 eV  445.50 nm  f=0.0000
     170 ->172         0.62289
     171 ->173         0.29319

 Excited State   3:   Singlet-AG     3.0285 eV  409.39 nm  f=0.0000
```

```
    170 ->172        -0.16877
    170 ->174        -0.16588
    171 ->173         0.54544
    171 ->175        -0.25524

Excited State   4:   Singlet-AU     3.2128 eV  385.91 nm  f=0.0757
    170 ->173        -0.33317
    170 ->175         0.26299
    171 ->174         0.54076

Excited State   5:   Singlet-AG     3.3671 eV  368.22 nm  f=0.0000
    170 ->172        -0.10087
    170 ->174         0.26452
    171 ->173         0.21902
    171 ->175         0.56182

Excited State   6:   Singlet-AU     3.3982 eV  364.85 nm  f=0.2992
    170 ->173         0.55461
    171 ->174         0.34811
    171 ->176         0.12557

Excited State   7:   Singlet-AU     3.6157 eV  342.91 nm  f=0.0038
    170 ->173        -0.11546
    170 ->175         0.10419
    170 ->177         0.23985
    171 ->176         0.62230

Excited State   8:   Singlet-AG     3.6560 eV  339.13 nm  f=0.0000
    170 ->174        -0.10972
    170 ->176         0.26411
    171 ->177         0.61193

Excited State   9:   Singlet-AU     3.7836 eV  327.69 nm  f=0.0155
    169 ->172        -0.10810
    170 ->175        -0.31317
    170 ->183         0.10813
    171 ->174         0.12050
    171 ->178         0.57310

Excited State  10:   Singlet-AG     3.7888 eV  327.24 nm  f=0.0000
    170 ->174         0.60896
    171 ->175        -0.31478
```